Photochemistry and Photobiology, 2022, 98: 347–353

Special Issue Research Article

Direct Detection of the Photorearrangement Reaction of Quinoline-Protected Dialkylanilines†

Runhui Liang[1,2], Xin Lan[2], Naeem Asad[3], Timothy M. Dore[3,4], Qidi Zhang[2], Lili Du[1,2]* and David Lee Phillips[2,5]*

[1]School of Life Sciences, Jiangsu University, Zhenjiang, China
[2]Department of Chemistry, The University of Hong Kong, Hong Kong, China
[3]New York University Abu Dhabi, Abu Dhabi, United Arab Emirates
[4]Department of Chemistry, University of Georgia, Athens, GA, US
[5]Guangdong-Hong Kong-Macao Joint Laboratory of Optoelectronic and Magnetic Functional Materials, Hong Kong, China

Received 16 September 2021, accepted 15 November 2021, DOI: 10.1111/php.13566

ABSTRACT

The photolysis reactions of (8-cyano-7-hydroxyquinolin-2-yl) methyl (CyHQ)-caged amines have been investigated using time-resolved spectroscopy methods. Unexpectedly, an unconventional Hofmann-Martius rearrangement reaction with high yield and regioselectivity occurred during the photolysis of some CyHQ-protected dialkylanilines (such as compounds 1a and 2a). To have more insights into the mechanism of this unexpected photorearrangement reaction, we characterized the reaction intermediates directly using time-resolved spectroscopy. Our new results showed that the anionic form of compound 1a was photoexcited to the singlet excited state, then a heterolytic cleavage of the C-N bond took place to give $CyHQ^+$ and the corresponding aniline. Thereafter, the recombined intermediate 6 was found to appear in about 19.7 and 44.3 ps for 1a (A) and 2a (A), respectively, before the generation of an *ortho*-substituted aniline (1b and 2b) via the excited-state deprotonation of 6. Thus, a logical photodynamic mechanism of this photoinduced Hofmann-Martius rearrangement reaction was deduced. This new insight into the reaction mechanisms may be helpful for the design of novel related photoactivatable aniline molecules and for understanding other similar photorearrangement reaction mechanisms.

INTRODUCTION

Photoremovable protecting groups (PPGs) are of increasing interest in the fields of photochemistry and photobiology and are employed as powerful tools for investigating physiological processes by encapsulating bioactive molecules or secondary messengers (1–4). A large variety of PPGs have been discovered for use in protecting and releasing various functional groups. To fully understand the criteria that govern the photorelease properties of selected PPGs, time-resolved techniques were employed to study the dynamics of the PPGs to find out the photocleavage pathways and reaction rates, the excited-state properties and so on (1,5,6), which had vital significance in expanding the current library of PPGs and the uncaged functional groups with desired properties and applications. Among the well-studied PPGs, the (8-cyano-7-hydroxyquinolin-2-yl)methyl (CyHQ) demonstrated outstanding properties: being stable toward spontaneous hydrolysis in the dark in simulated physiological buffer solution, sufficiently sensitive to both one- and two-photon excitation, and working well in living organism (5,7–9).

The photoactivation of different functional groups and biological compounds (including tamoxifen, 4-hydroxytamoxifen, and mifepristone analogs) caged by CyHQ were proven to be successful. On the other hand, aryl alkyl ammonium salts of CyHQ generated a corresponding *ortho*-substituted dialkylaniline after photoexcitation via an unconventional photorearrangement reaction, instead of releasing the corresponding aniline (Scheme 1) (5,10). This reaction was observed in a series of CyHQ-protected anilines (**1a** and **2a** as examples), which generated the rearranged products in high regioselectivity (**1b** and **2b**): only *ortho*-substituted dialkylanilines were found and confirmed by ^{1}H, ^{13}C, DEPT-135°, and two-dimensional NMR spectra. Moreover, the rearranged products of **1a** and **2a** were characterized by HPLC and the product yields were high (85% and 95%, respectively) (10). This Hofmann-Martius type photorearrangement reaction of *N*-alkylanilines with such high yields and regioselectivity have rarely been reported. The first report on the rearrangement of an *N*-alkylanilines reaction was published by Hofmann *et al*. (11,12), and the reaction required harsh conditions (catalyzed by hydrohalides at a high temperature) and had low product yield and regioselectivity. However, the solid-state Hofmann-Martius rearrangement reaction mainly gave *ortho*-alkylated products, because the diffusion process was inhibited in the solid state (13). Several groups carried out mechanistic investigations of the thermal transformation of acid-catalyzed *N*-alkylanilines into ring-alkylated aniline at the *ortho*- or *para*-position of the aniline ring,

*Corresponding author emails: dulili@ujs.edu.cn (Lili Du), phillips@hku.hk (David Lee Phillips)
†This article is part of a Special Issue dedicated to the topic of Emerging Developments in Photocaging.
Runhui Liang and Xin Lan contributed equally to this work.

which revealed two main steps of the rearrangement reaction: the dissociation of *N*-alkylaniline hydrohalide into two parts after heating at high temperature and the intermolecular alkylation of the dissociated components (14–16). The form of the migrating alkyl group was still obscure and species considered included radicals (15), olefins (14), or carbocation species (14). The rearrangement reactions of *N*-alkylanilines by UV irradiation were also reported, while the *ortho*/*para*-isomer ratio of the products was not high (ca. 2–3) unless done for the *para*-blocked aniline (17,18). Still, little was known about the mechanism of the Hofmann-Martius photorearrangement reaction, particular for the photorearrangement reaction of CyHQ-protected *N*-alkylanilines with high yield and regioselectivity. Scheme 2 shows a proposed mechanism of the photorearrangement reaction of CyHQ-protected *N*-alkylanilines, where heterolytic cleavage of the C-N bond takes place.

CyHQ-protected tertiary amines **1a** and **2a** were reported to mainly undergo the photorearrangement pathway, whereas **3a** adopted the photolysis mechanism (Scheme 1 and Fig. 1). It is of fundamental meaning to decipher the underlying photorearrangement mechanism and compare it with the mechanism of the photolysis reaction of the CyHQ-protected compounds. UV-vis absorption and resonance Raman (RR) spectroscopies together with quantum chemical stimulations were used to determine the ground-state properties of the molecule. In addition, the excited-state dynamics after light irradiation were further elucidated by employing femtosecond and nanosecond time-resolved transient absorption spectroscopies (fs-TA and ns-TA). The same methodologies were also applied to study the photodynamics of *N*-((8-cyano-7-hydroxyquinolin-2-yl)methyl)-*N*,*N*-diethylethanaminium methanesulfonate (CyHQ-TEA) thoroughly, and the heterolytic C-N bond cleavage was found to take place in about 70 ps in the singlet excited state (5). CyHQ-TEA was used as a model compound to help analyze the ultrafast photophysical and photochemical mechanisms of the compounds examined here. To the best of our knowledge, this is the first time to delve into the mechanism of a Hofmann-Martius photorearrangement reaction in CyHQ-protected dialkylaniline with direct time-resolved spectroscopic observation. The comparison of the comprehensive mechanisms of the photorearrangement and photolysis reactions will further shed light on the molecular design for photorearrangement of aniline with high yield and desired regioselectivity.

MATERIALS AND METHODS

Materials. The synthesis and characterization of **1a**, **2a**, **3a**, and CyHQ-TEA and the product analysis of their photochemistry were reported previously (5,10).

Fs-TA experiments were performed on a commercial Helios pump-probe transient absorption spectroscopy system (Ultrafast Systems), a detailed description of which was reported previously (19,20). Briefly, a femtosecond regenerative amplified Ti:Sapphire laser system generated the amplified 150 fs laser pulses (λ = 800 nm) that were split into a pump beam and a probe beam. The pump laser beam was adjusted to 267 nm (the third harmonic of 800 nm) and the probe beam passed through a CaF_2 crystal to generate a white-light continuum (325–650 nm). The 50 mL sample solutions with an absorbance of ~1 at 267 nm were prepared in a flowing 2-mm path-length quartz cuvette to avoid the accumulation of photodecomposition products.

Ns-TA experiments were conducted on an LP920 laser flash spectrometer (Edinburgh Instruments Ltd.) with an instrumental set-up and methods as described in previous work (19,20). Briefly, a white-light continuum (280–800 nm) used as a probe light source was obtained from a 450 W ozone free Xe arc lamp and a Q-switched Nd:YAG laser (the fourth harmonic line at λ = 266 nm) was employed as the pump laser source. The 50 mL sample solutions with an absorption of ~1 at 266 nm were prepared in a flowing 1 cm path-length quartz cuvette. After the samples were photoexcited by a 266 nm laser beam, the probe light passed through the solution at a right angle. The transmitted signals were collected by a photomultiplier detector (for the kinetics mode) or an array detector (for the spectral mode).

RR experiments were achieved on a home-made set-up that was described previously (21). In the present experiments, the 266-nm laser pulse (around 2 mW) produced from the fourth harmonic of an Nd:YAG nanosecond pulsed laser was used as the probe beam to photoexcite the flowing sample solutions. The Raman scattered signal was collected by a liquid-nitrogen-cooled charge-coupled device (CCD) detector using a backscattering geometry. The Raman bands of ACN were used to calibrate the Raman shifts with an estimated uncertainty of 5 cm^{-1}. The 50 mL solutions with absorbance of ~1 at 266 nm in a 2-mm path-length cuvette were prepared for use in the experiments.

Computational methods. Density functional theory/time-dependent density functional theory (DFT/TD-DFT) calculations employing the B3LYP method and the 6-311G** basis set and using a CPCM solvation model of water were calculated using the Gaussian09 (22) software suite installed on a high-performance computing cluster at the University of Hong Kong. The calculated Raman spectra were obtained using a Lorentzian function with a 10-cm^{-1} bandwidth for the vibrational frequencies together with a scaling factor of 0.99. The calculated absorption spectra of **1a (A)** and **1a (N)** were done using TD-DFT calculations and the electronic absorption spectra were estimated by GaussSum software using a half band width of 2500 cm^{-1} (23).

RESULTS AND DISCUSSION

UV-vis absorption and RR spectroscopies

The photochemical reactions of CyHQ-protected anilines take place in aqueous solutions at pH 7.2. To identify whether the neutral or anionic form of the CyHQ-protected anilines initiate the photochemical reactions, UV-vis absorption and RR spectroscopies of **1a** in different solutions were compared with the simulated spectra (Fig. 2 and Figure S1). The lowest absorption band and the strongest absorption band appeared at 380 and 249 nm in an aqueous buffer solution (ACN/PBS v/v = 1:1, pH 7.2) and at 338 and 230 nm in a pure ACN solution individually

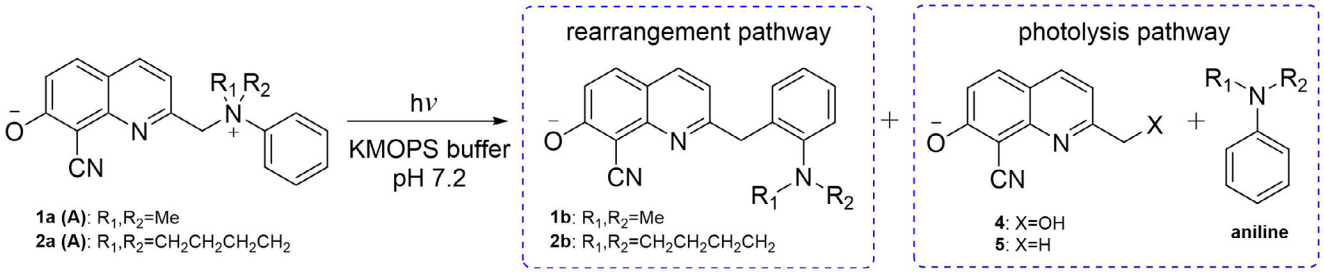

Scheme 1. Photoreactions of **1a** and **2a** in KMOPS [KCl 100 mM, 3-(N-morpholino) propanesulfonic acid 10 mM, pH 7.2] buffer solution following 365 nm photoexcitation.

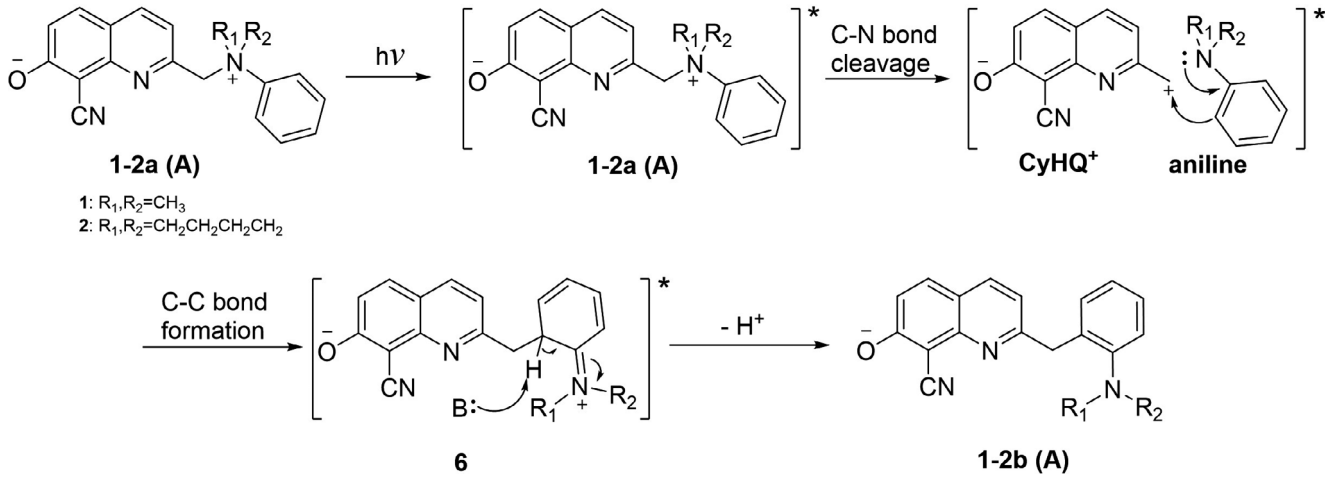

Scheme 2. Proposed mechanism for the Hofmann-Martius photorearrangement reaction.

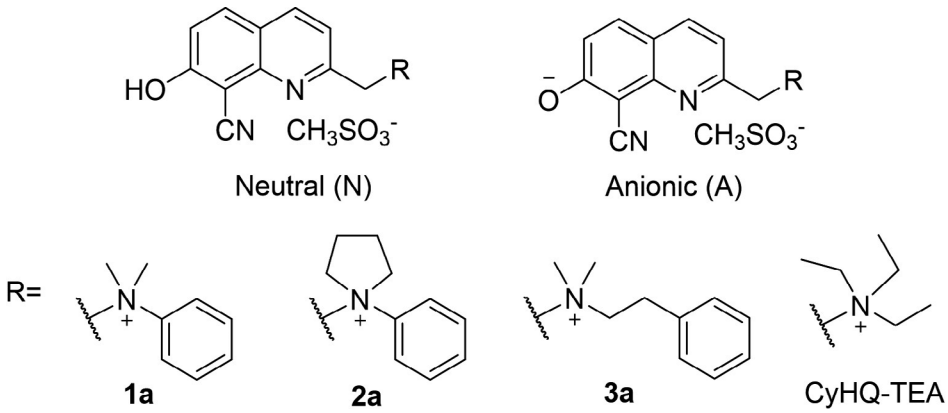

Figure 1. Chemical structures of selective 8-cyano-7-hydroxyquinolinyl (CyHQ) salts of tertiary amines in anionic (A) and neutral (N) forms.

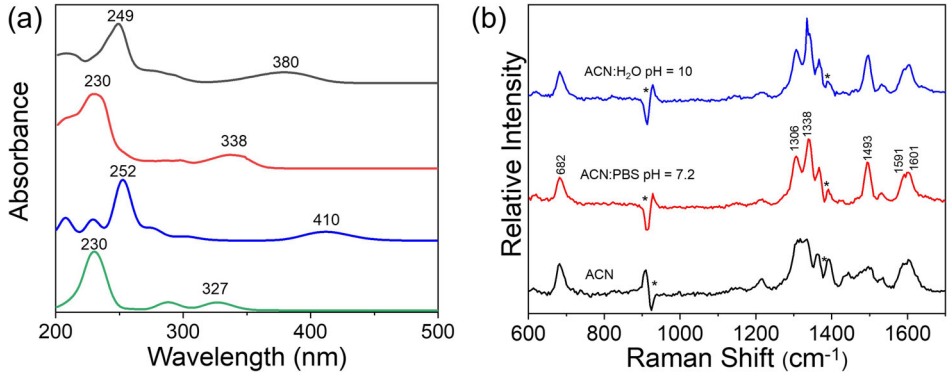

Figure 2. (a) Comparison of UV-vis absorption spectra of **1a** in ACN/PBS (v/v = 1:1 pH 7.2) solution (black) and in ACN solution (red) with the calculated absorption spectra of deprotonated **1a** (blue) and its neutral form (green); (b) Resonance Raman spectra of **1a** in various solutions with 266 nm excitation at room-temperature. Solvent subtraction is marked as * in the spectra.

(Fig. 2a). Similar absorption bands were also observed in the simulated absorption spectra of **1a (A)** and **1a (N)**. Moreover, CyHQ-OAc showed a similar absorption pattern as **1a** with its lowest energy absorption peaks at 330 nm (pure ACN) and 364 nm (neutral buffer solution), which were attributed to the absorption of the neutral and anionic forms, respectively. The much more facile deprotonation of the CyHQ molecules compared to other 8-substituted-7-hydroxyquinolines appears due to the presence of the strong electron-withdrawing effect by the 8-cyano group (pK_a of CyHQ-OAc was 4.9) (24,25). Therefore, similar to the assignment of CyHQ-OAc, the absorption bands at 338 and 380 nm of **1a** were mainly corresponding to the phenolic (neutral) and phenolate (anionic) forms, respectively. The red-shifting of the absorption peaks in the buffer solution indicated that a deprotonation process of **1a** occurred in the buffer solutions in the ground state.

Resonance Raman spectroscopy was used to provide more precise assignments by giving fingerprint vibrational frequency information. As shown in Fig. 2b, the anionic form of **1a** mainly existed in the mixed aqueous solution at a high pH value (ACN/H_2O v/v = 1:1, pH 10, made more basic by adding some NaOH) (Fig. 2b). Compound **1a** demonstrated that the vibrational Raman shifts in near neutral aqueous buffer solution are similar to those seen in the basic solution with obvious Raman bands at 682, 1306, 1338, 1493, 1591, 1601 cm^{-1}. Thus, **1a** mainly exists as the phenolate form in the near neutral buffer solution, which was in line with the UV-vis absorption results. Moreover, the calculated Raman spectra of **1a (N)** and **1a (A)** (Figure S1) were similar to the experimental data in ACN and ACN/PBS solution, respectively. This further confirmed that **1a** was deprotonated in the near neutral buffer solutions in the ground state and the photochemical reaction was initiated by the anionic form of the molecule. The absence of the phenolic form of **1a** in neutral aqueous solution is probably because of the lower pK_a of the phenol induced by the strongly electron-withdrawing nature of the 8-cyano substituent group.

TA spectroscopies

To explore the ultrafast photoinduced C–N bond cleavage and rearrangement mechanism of **1a** and **2a** in aqueous solutions, fs-TA spectroscopy was employed to detect the short-lived intermediates involved in the reaction. As discussed above, **1a (A)** was the main form of the ground state in neutral aqueous solutions. Upon 267 nm irradiation, a characteristic transient absorption profile that is similar to the lowest singlet excited state (S_1) of CyHQ-TEA (A) was gradually produced from 0.4 to 1.2 ps with excited-state absorption (ESA) bands at 336, 411, and 630 nm together with a stimulated emission (SE) band at 472 nm (Fig. 3a). This process could be reasonably assigned to the internal conversion process of **1a (A)** from a higher singlet excited state (S_n) to the S_1 excited state. Subsequently, two strong ESA bands at 336 and 630 nm decreased dramatically and the band at 411 nm red shifted to 415 nm with decreased intensity in the period from 1.2 to 6.31 ps (Fig. 3b). However, the SE band showed a slight blue-shifting in this time delay range, which probably implied a heterolytic C–N cleavage reaction from the S_1 excited state of **1a (A)** (5). Two obvious processes were observed in Fig. 3c: three ESA bands depopulated in intensity simultaneously until 30 ps; after 30 ps, the ESA band at 630 nm kept decreasing, while a small red-shifting was observed in the band from 336 nm to 342 nm. Eventually, three ESA bands located at 342, 423 and 540 nm were clearly seen at the 2.3-ns time delay (Fig. 3c), which agreed well with the calculated transitions of the S_1 excited state of **6** (Table S1). Thus, these two processes corresponded to the production of the S_1 excited state of **6** (Scheme 2) and its deprotonation to generate **1b** (**A**). The ns-TA spectra were almost unchanged until 5 ms and correlated well with the steady-state UV-vis absorption spectrum of the product **1b (A)** after the photorearrangement reaction (Figure S2a) and the kinetics were not affected by oxygen (Figure S2b,c). Therefore, the spectra observed in the ns-TA were mainly attributed to the absorption of the ground-state product **1b (A)**.

Kinetic analyses were conducted on the characteristic absorption bands at 340 and 630 nm with exponential fitting functions. Three similar time constants (0.3, 2.5, and 19.7 ps) were obtained from the 340 and 630 nm bands, whereas a fourth time constant (>3 ns) was only obtained by fitting the 630 nm band. Taken together with the TA spectral analysis, the 0.3, 2.5 and 19.7 ps time constants were attributed to the production of S_1 excited state of **1a (A)**, the photolysis process to generate $CyHQ^+$, and the formation of the S_1 excited state of **6**, respectively. The fourth time constant (>3 ns) was assigned to the formation of **1b (A)** by deprotonation.

The photorearrangement reaction was also observed for **2a** with a higher product yield (95%) than **1a** (85%) (10). We also

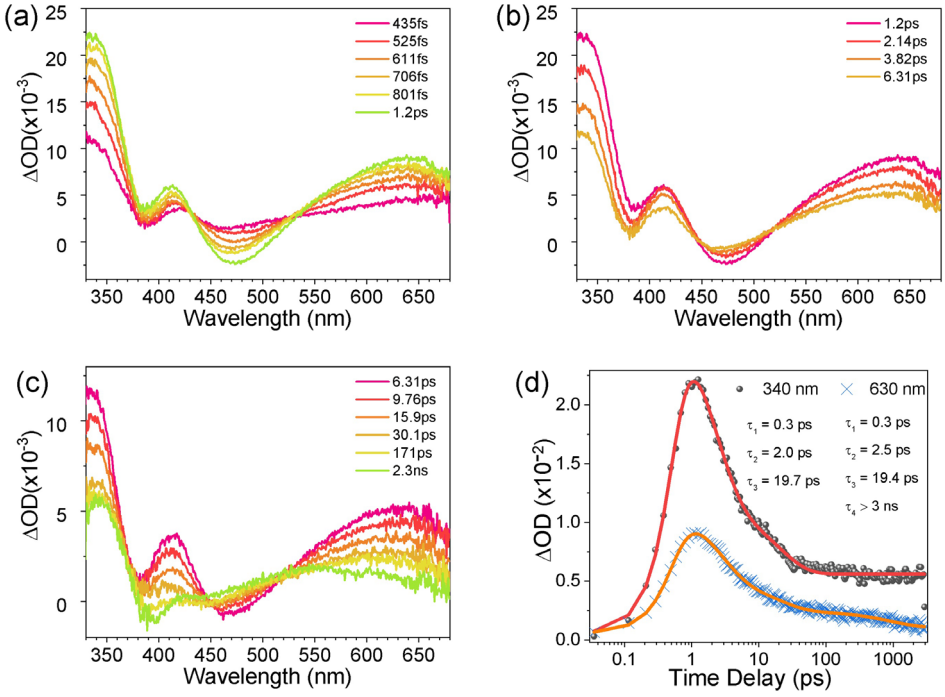

Figure 3. (a–c) fs-TA spectra of **1a** after 267 nm photoexcitation in ACN/PBS (v/v = 1:1, pH 7.2) solution at various time delay ranges; (d) kinetics at 340 and 630 nm (solid lines indicate the best fit of the experimental data).

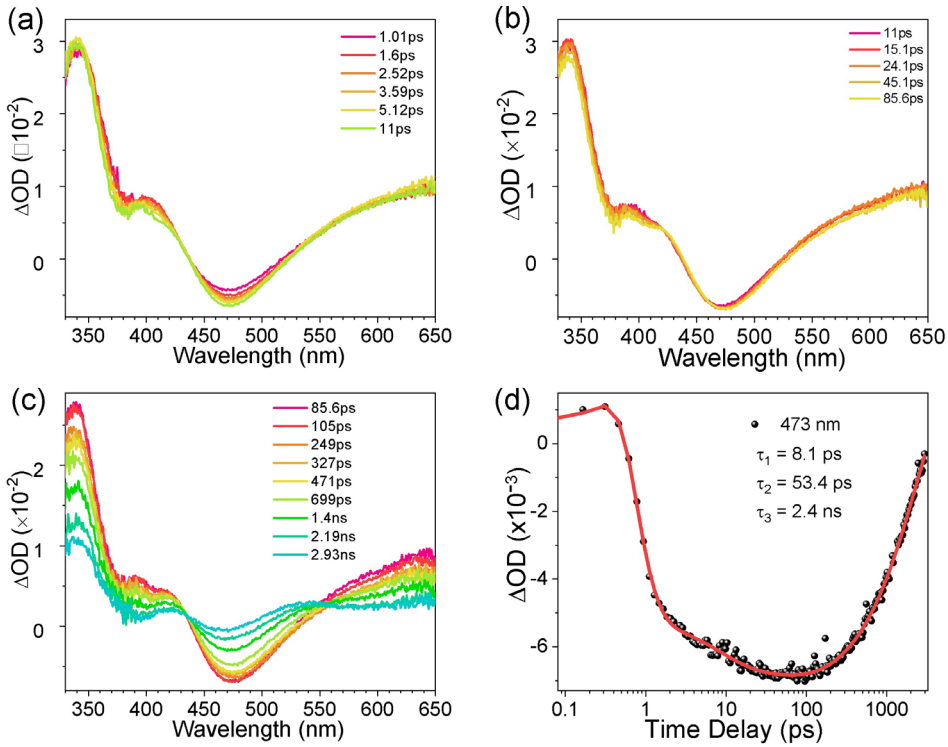

Figure 4. (a–c) fs-TA spectra of **3a** after 267 nm photoexcitation in ACN/PBS (v/v = 1:1, pH 7.2) solution at various time delay ranges; (d) kinetics at 475 nm (solid line indicates the best fit of the experimental data).

employed fs-TA to investigate the ultrafast photochemical and photophysical dynamics of **2a**. Not surprisingly, the fs-TA spectra of **2a** after 267 nm photoexcitation in mixed ACN/PBS (v/v = 1:1, pH 7.2) solution were similar to those observed for **1a** (Figure S3). The same photodynamic processes were observed for **2a**, and the lifetimes of these processes were in line with those of **1a** as well: 0.2 ps (production of vibrationally cooled S_1 excited state), 3.7 ps (C–N bond cleavage), 44.3 ps (C–C bond formation), and >3 ns (formation of the rearranged product **2b (A)**).

Unlike **1a** and **2a**, **3a** mainly underwent the photolysis pathway to release product **4** and its corresponding amine after irradiation, which was similar with the reported results for CyHQ-TEA (5). Although the ESA profiles of **1a** and **3a** were similar, there were two differences in the two spectra (Fig. 4). Firstly, the SE band reached its maximum at 1.2 ps for **1a** (Fig. 3a), whereas for **3a**, it continually decreased from 1 to 11 ps and remained at the same intensity until 85.6 ps. Secondly, unlike **1a**, **3a** presented a clear peak at 340 nm and a band tail at 650 nm. With the solid evidence of the SE band and the spectral reference from CyHQ-TEA (5), the initial TA spectra (Fig. 4a) was assigned to the generation of the S_1 excited state of **3a (A)**. After 85.6 ps, the intense band at 340 nm declined dramatically together with the disappearance of the broad band tail at 650 nm, and the SE band decayed with a small blue-shifting. Two isosbestic point at 440 and 550 nm were clearly observed, which indicated a conversion of different species. The spectral changes of **3a** were similar with those of CyHQ-TEA (5), thus the photodynamic pathways of **3a** were assigned the same way as for CyHQ-TEA, which were the generation of the S_1 excited state of **3a (A)**, a C–N bond cleavage, and an inter-system crossing (ISC) of $CyHQ^+$, and the time constants of each of these processes were determined to be 8.1, 53.4, and 2400 ps, respectively. The decay of the triplet excited state of $CyHQ^+$ was further traced by ns-TA (Figure S4), and the prolonged lifetime (7 μs) in an argon-purged solution confirmed the existence of a triplet excited state of $CyHQ^+$, which then reacted with water to generate photolysis product **4**.

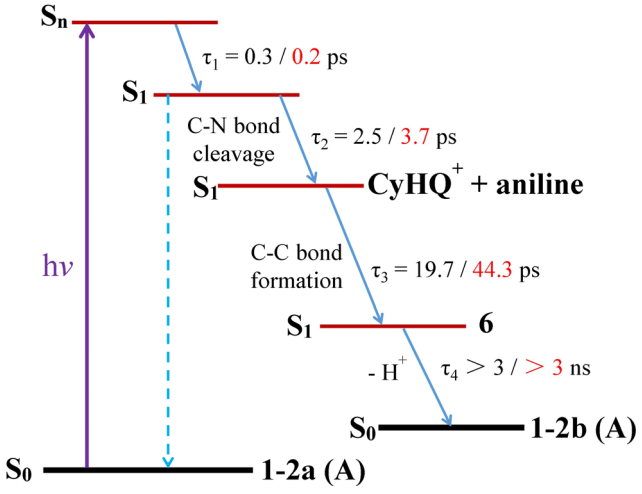

Scheme 3. Proposed deactivation and photochemical reaction pathways for **1a (A)** and **2a (A)** in buffer aqueous solution and the time constants colored in black and red are represented for **1a** and **2a**, respectively.

CONCLUSION

A comprehensive mechanistic study of the CyHQ salts of tertiary amines with different photochemical dynamics (photorearrangement and photolysis) was conducted by using UV-vis absoprtion

and transient absorption spectroscopy methods together with results from RR experiments and quantum chemical calculations. The CyHQ salts could deprotonate easily in neutral buffer aqueous solution due to the low pK_a of the parent compounds and mainly existed as the anionic form in aqueous neutral buffer solutions. Upon photoexcitation, the heterolysis of the C–N bond took place for all of the CyHQ-protected compounds, giving a $CyHQ^+$ and aniline/amine from the S_1 excited state. In the Hofmann-Martius photorearrangement mechanism, the released $CyHQ^+$ recombined with the *ortho*-position of the aniline to produce the rearranged intermediate **6** within 19.7 and 44.3 ps for **1a** and **2a**, respectively (Scheme 3). However, in the photolysis pathway (exemplified by **3a**), the released $CyHQ^+$ went on to form the triplet excited state via ISC in 2.4 ns and subsequently reacted with water to generate the product **4** (Scheme S1). These two reactions were highly selective and negligible amounts of byproducts were found. This can have great importance for the synthesis of *ortho*-substituted anilines and the photorelease of bioactive amines for use in physiological experiments.

Acknowledgements—This work was supported by grants from the Hong Kong Research Grants Council (GRF 17302419), The University of Hong Kong Development Fund 2013-2014 project "New Ultrafast Spectroscopy Experiments for Shared Facilities", the National Science Fund of China (21803026), Natural Science Foundation of Jiangsu Province (BK20180854), Major Program of Guangdong Basic and Applied Research (2019B030302009), Guangdong-Hong Kong-Macao Joint Laboratory of Optoelectronic and Magnetic Functional Materials (2019B121205002), and NYU Abu Dhabi.

CONFLICT OF INTEREST

The authors declare no competing financial interests.

SUPPORTING INFORMATION

Additional supporting information may be found online in the Supporting Information section at the end of the article:

Figure S1. Resonance Raman spectra of 1a in mixed ACN/PBS (v/v = 1:1, pH 7.2) solution with 266 nm excitation at room-temperature (top) and the calculated Raman spectra of **1a (A)** (middle) and **1a (N)** (bottom) based on B3LYP/6-311G (d,p) level of theory. Solvent subtraction is marked as *.

Figure S2. (a) ns-TA spectra of 1a in ACN/PBS (v/v = 1:1, pH 7.2) solution upon 266 nm photoexcitation at various delay times. (b, c) The kinetics of the characteristic absorption band observed at 350 nm of 1a (black circles) in open air and in O_2 saturated solutions, respectively. The solid lines indicate the fitting to the experimental data. (d) ns-TA spectra of 2a in ACN/PBS (pH 7.2) solution upon 266 nm photoexcitation at various delay times. (e, f) Kinetics of the characteristic absorption band observed at 350 nm of 2a (black circles) in open air and O_2 saturated solutions, respectively. The solid lines indicate the fitting to the experimental data.

Figure S3. (a–c) fs-TA spectra of 2a after 267 nm photoexcitation in ACN/PBS (v/v = 1:1, pH 7.2) solution at various time delay ranges, (d) kinetics at 340 and 630 nm (solid lines indicate the best fitting of the experimental data).

Figure S4. (a) ns-TA spectra of 3a in ACN/PBS (v/v = 1:1, pH 7.2) solution upon 266 nm photoexcitation at various delay times. (b) The kinetics of the characteristic absorption band observed at 528 nm of 3a in an argon-purged solution and open air (inserted) conditions, respectively. The solid lines indicate the fitting to the experimental data.

Table S1. The calculated wavelength (λ) and oscillator strength (f) of selective transitions for the S0 and S1 states of 6 are shown, and the TD-DFT calculation is based on the B3LYP/6-311G** level of theory.

Scheme S1. Proposed deactivation and photochemical reaction pathways of 3a in buffer solution.

Data S1. Optimized structural coordinates.

REFERENCES

1. Zhu, Y., C. M. Pavlos, J. P. Toscano and T. M. Dore (2006) 8-Bromo-7-hydroxyquinoline as a photoremovable protecting group for physiological use: mechanism and scope. *J. Am. Chem. Soc* **128**, 4267–4276.
2. Klan, P., T. Solomek, C. G. Bochet, A. Blanc, R. Givens, M. Rubina, V. Popik, A. Kostikov and J. Wirz (2013) Photoremovable protecting groups in chemistry and biology: reaction mechanisms and efficacy. *Chem. Rev* **113**, 119–191.
3. Pelliccioli, A. P. and J. Wirz (2002) Photoremovable protecting groups: Reaction mechanisms and applications. *Photochem. Photobiol. Sci* **1**, 441–458.
4. Ellis-Davies, G. C. (2007) Caged compounds: Photorelease technology for control of cellular chemistry and physiology. *Nat. Meth.* **4**, 619–628.
5. Asad, N., D. Deodato, X. Lan, M. B. Widegren, D. L. Phillips, L. Du and T. M. Dore (2017) Photochemical activation of tertiary amines for applications in studying cell physiology. *J. Am. Chem. Soc.* **139**, 12591–12600.
6. Ma, J., J. M. Mewes, K. T. Harris, T. M. Dore, D. L. Phillips and A. Dreuw (2017) Unravelling the early photochemical behavior of (8-substituted-7-hydroxyquinolinyl)methyl acetates through electronic structure theory and ultrafast transient absorption spectroscopy. *Phys. Chem. Chem. Phys.* **19**, 1089–1096.
7. O'Connor, M. J., L. L. Beebe, D. Deodato, R. E. Ball, A. T. Page, A. J. VanLeuven, K. T. Harris, S. Park, V. Hariharan, J. D. Lauderdale and T. M. Dore (2019) Bypassing glutamic acid decarboxylase 1 (Gad1) induced craniofacial defects with a photoactivatable translation blocker morpholino. *ACS Chem. Neurosci.* **10**, 266–278.
8. McLain, D. E., A. C. Rea, M. B. Widegren and T. M. Dore (2015) Photoactivatable, biologically-relevant phenols with sensitivity toward 2-photon excitation. *Photochem. Photobiol. Sci.* **14**, 2151–2158.
9. Hennig, A. K., D. Deodato, N. Asad, C. Herbivo and T. M. Dore (2020) Two-photon excitable photoremovable protecting groups based on the quinoline scaffold for use in biology. *J. Org. Chem.* **85**, 726–744.
10. Deodato, D., N. Asad and T. M. Dore (2019) Photorearrangement of quinoline-protected dialkylanilines and the photorelease of aniline-containing biological effectors. *J. Org. Chem.* **84**, 7342–7353.
11. Hofmann, A. W. (1871) Methylirung der Phenylgruppe im Anilin. *Ber. Dtsch. Chem. Ges* **4**, 742–748.
12. Hofmann, A. W. (1872) Umwandlung des Anilins in Toluidin. *Ber. Dtsch. Chem. Ges* **5**, 720–722.
13. Site, A. D. (1966) Thermal decomposition of trimethylphenylammonium iodide in the solid state. *J. Org. Chem.* **31**, 3413–3415.
14. Hart, H. and J. R. Kosak (1962) Mechanism of rearrangement of N-alkylanilines. *J. Org. Chem* **27**, 116–121.
15. Drumm, P. J., W. F. O'Connor and J. Reilly (1940) The molecular rearrangement of tertiary aryl alkyl anilines. *J. Am. Chem. Soc.* **62**, 1241–1243.
16. Hickinbottom, W. J. (1934) The rearrangement of the alkylanilines. Part VI. Mechanism of the rearrangement. *J. Chem. Soc. (resumed).* 1700–1705.
17. Ogata, Y. and K. Takagi (1970) Photochemical reactions of N-alkylanilines. *J. Org. Chem* **35**, 1642–1945.

18. Ogata, Y. and K. Takagi (1971) Photochemical rearrangement of N-substituted benzylanilines. *Bull. Chem. Soc. Jpn* **44**, 2186–2191.
19. Liang, R., W. Xiong, X. Bai, L. Du and D. L. Phillips (2021) Direct observation of the triplet excited states and dynamics of platinum (II)-tetraphenylethylene complexes by time-resolved transient absorption spectroscopy. *J. Phys. Chem. C* **125**, 11432–11439.
20. Du, L., M. D. Li, Y. Zhang, J. Xue, X. Zhang, R. Zhu, S. C. Cheng, X. Li and D. L. Phillips (2015) Photoconversion of beta-lapachone to alpha-lapachone via a protonation-assisted singlet excited state pathway in aqueous solution: A time-resolved spectroscopic study. *J. Org. Chem* **80**, 7340–7350.
21. Li, M. D., C. S. Yeung, X. Guan, J. Ma, W. Li, C. Ma and D. L. Phillips (2011) Water- and acid-mediated excited-state intramolecular proton transfer and decarboxylation reactions of ketoprofen in water-rich and acidic aqueous solutions. *Chem. Eur. J* **17**, 10935–10950.
22. Frisch, M. J., G. W. T, H. B. Schlegel, G. E. Scuseria, M. A. Robb, J. R. Cheeseman, G. Scalmani, V. Barone, B. Mennucci, G. A. Petersson, H. Nakatsuji, M. Caricato, X. Li, H. P. Hratchian, A. F. Izmaylov, J. Bloino, G. Zheng, J. L. Sonnenberg, M. Hada, M. Ehara, K. Toyota, R. Fukuda, J. Hasegawa, M. Ishida, T. Nakajima, Y. Honda, O. Kitao, H. Nakai, T. Vreven, J. A. Jr Montgomery, J. E. Peralta, F. Ogliaro, M. Bearpark, J. J. Heyd, E. Brothers, K. N. Kudin, V. N. Staroverov, T. Keith, R. Kobayashi, J. Normand, K. Raghavachari, A. Rendell, J. C. Burant, S. S. Iyengar, J. Tomasi, M. Cossi, N. Rega, J. M. Millam, M. Klene, J. E. Knox, J. B. Cross, V. Bakken, C. Adamo, J. Jaramillo, R. Gomperts, R. E. Stratmann, O. Yazyev, A. J. Austin, R. Cammi, C. Pomelli, J. W. Ochterski, R. L. Martin, K. Morokuma, V. G. Zakrzewski, G. A. Voth, P. Salvador, J. J. Dannenberg, S. Dapprich, A. D. Daniels, O. Farkas, J. B. Foresman, J. V. Ortiz, J. Cioslowski & D. J. Fox (2013) Gaussian 09, Revision D.01.
23. O'Boyle, N. M., A. L. Tenderholt and K. M. Langner (2008) cclib: A library for package-independent computational chemistry algorithms. *J. Comput. Chem* **29**, 839–845.
24. An, H. Y., C. Ma, W. Li, K. T. Harris, T. M. Dore and D. L. Phillips (2010) Resonance Raman characterization of the different forms of ground-state 8-substituted 7-hydroxyquinoline caged acetate compounds in aqueous solutions. *J. Phys. Chem. A* **114**, 2498–2505.
25. Davis, M. J., C. H. Kragor, K. G. Reddie, H. C. Wilson, Y. Zhu and T. M. Dore (2009) Substituent effects on the sensitivity of a quinoline photoremovable protecting group to one- and two-photon excitation. *J. Org. Chem* **74**, 1721–1729.